Solvent dependent nuclearity of manganese complexes with a polydentate hydrazone-based ligand and thiocyanate anions

Ghodrat Mahmoudi [a,*], Ennio Zangrando [b], Werner Kaminsky [c], Piotr Garczarek [d], Antonio Frontera [e,*]

[a] Department of Chemistry, Faculty of Science, University of Maragheh, P.O. Box 55181-83111, Maragheh, Iran
[b] Department of Chemical and Pharmaceutical Sciences, University of Trieste, Via L. Giorgieri 1, 34127 Trieste, Italy
[c] X-ray Crystallography Laboratory, University of Washington, Box 351700, Seattle, WA 98195-1700, USA
[d] Faculty of Chemistry, Wroclaw University of Technology, 27 Wybrzeze Wyspianskiego Street, 50-370 Wroclaw, Poland
[e] Department of Chemistry, Universitat de les Illes Balears, Crta. de Valldemossa, km 7.5, 07122 Palma de Mallorca (Baleares), Spain

ARTICLE INFO

Article history:
Received 17 August 2016
Received in revised form 15 October 2016
Accepted 19 October 2016
Available online 20 October 2016

Keywords:
Manganese
Complex nuclearity
Crystal engineering
Self-assembly
Solvent effect

ABSTRACT

The reaction of Mn(II) chloride with the 2-benzoylpyridyl-(2-picolyl)-hydrazone ligand (HL) and thiocyanate anions in different solvent systems affords mono- $[Mn(HL)_2(SCN)_2]$ (**1**), di- $[Mn_2(HL)_2(SCN)_4]$ (**2**) and a tetra-nuclear complex $[Mn_4(L)_4(SCN)_4]\cdot 2(CH_3CN)$ (**3**) with concomitant different coordination modes of the ligands. Remarkably, the nuclearity of the complexes only depends on the solvent used, ethanol for **1**, *n*-propanol for **2** and acetonitrile for **3**. The complexes have been characterized by elemental analysis, IR spectroscopy technique and the molecular structures determined by single crystal X-ray analysis. In **1** and **2** the ligands are present in its neutral form, while they are deprotonated in **3**, but more significantly in all structures a different denticity of ligands was detected: in complex **1** one molecule is tridentate coordinated though the N,N,O donor set, the other bidentate through N,O; in **2** the ligands are N,N,O-tridentate; finally in **3** each ligand, acting as N,N,O,N-tetradentate species, bridges two metals to form a tetranuclear assembly. The crystal structures have been described using the Hirshfeld surface analysis. Finally, we have studied the ability of the thiocyanato ligand to participate in H-bonding and C—H/π interactions by means of DFT calculations (B3LYP/6-31+G**).

1. Introduction

In the past decades the design and synthesis of coordination polymers and metal-organic frameworks (MOFs) have attracted a wide interest by researchers. Polydentate Schiff base ligands allow synthesis of coordination compounds which are widely investigated not only for their interesting structure and stereochemistry, but also for their tunable coordination fashions under different experimental conditions, and for the formation of polynuclear derivatives [1] In this field hydrazone compounds bearing pyridine rings that increase the denticity of the ligands have been often used. The coordination versatility of these molecules provides the possibility to form different complexes with various transition metals, such as mononuclear [2], polynuclear ones [3], and also copper 'chain' complexes [4], of intriguing structure and property. Thus the ligand flexibility combined with its donor rich nature leads to a condition such that, in addition to conformational variations, different structural motifs can be achieved (Scheme 1).

However, the influence of solvent in the formation of metal complexes and coordination polymers is still relatively poorly understood and systematic studies on this subject is matter of interest to scientists [5]. This approach is attractive because bridging ligands can potentially be arranged around the metal centers in diverse ways, and therefore, can result in a variety of complex structures. Moreover, if the arrangement of a ligand in the coordination could be changed by the variation of synthesis conditions such as the solvent system, different coordination polymer species could be selectively afforded from the same components. In many previous examples, solvent molecules were found to produce a dramatic effect on the extended structure of the network by acting as a coordination ligand or a template for the assembly [6].

In this respect the multidentate Schiff base ligand *2-phenylpyridine piconyl hydrazone* (HL) represents potential for its different hapticity also modulated by deprotonation of amide NH group being able to form coordination polymers with the adoption of different conformations. By using this ligand and SCN anions, in the present work we report three novel Mn(II) complexes, namely a

* Corresponding authors.
E-mail addresses: mahmoudi_ghodrat@yahoo.co.uk (G. Mahmoudi), toni.frontera@uib.es (A. Frontera).

http://dx.doi.org/10.1016/j.ica.2016.10.028

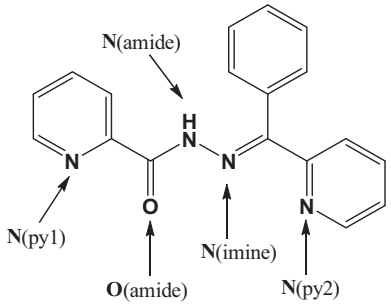

Scheme 1. Structure of the 1-(phenyl(pyridin-2-yl)methylene)pyridine-2-carbohydrazide) ligand used in this work.

mono- $[Mn(HL)_2(SCN)_2]$ (**1**), a di- $[Mn_2(HL)_2(SCN)_4]$ (**2**) and a tetranuclear complex $[Mn_4(L)_4(SCN)_4]\cdot 2(CH_3CN)$ (**3**), obtained by using different solvent systems in the synthetic strategy (Scheme 2). By using DFT calculations (B3LYP/6-31G*) and Hirshfeld surface analysis, we have also studied the interesting supramolecular assemblies found in the solid state of compounds **1**–**3**. We have focused our attention to the ability of the thiocyanato ligand to participate in "unconventional" C—H/π interactions and to influence the crystal packing of **1**–**3**. Recently, the ability of N/S ends of the pseudohalide ligand to establish H-bonding interactions has been used to explain the ambidentate behaviour of the thiocyanato ligand [7]. Furthermore, its ability to participate in other interactions like "unconventional" C—H/π interactions involving the π-system of the pseudohalide ligand has been also used to explain the stability of the N-bonded and S-bonded compounds [8].

2. Experimental

2.1. Materials and general methods

All the reagents were purchased commercially and used as received without further purification. The Schiff base was prepared following the reported method as described elsewhere [9] and used without further purification. The FT-IR spectra (4000–400 cm^{-1} region) were recorded from KBr pellets with a Bruker Tensor 27 spectrometer. Microanalyses were performed using a Heraeus CHN-O-Rapid analyzer.

2.1.1. Synthesis of $[Mn(HL)_2(SCN)_2]$ (**1**)

$MnCl_2\cdot 4H_2O$ (0.10 g, 0.50 mmol), KSCN (0.097 g, 1.0 mmol) and (0.302 g, 1.0 mmol), were placed in the main arm of a branched tube. Ethanol was carefully added to fill the arms. The tube was sealed and immersed in an oil bath at 60 °C while the branched arm was kept at ambient temperature. After 5 days, crystals of **1** isolated in the cooler arm were filtered off, washed with acetone and ether, and dried in air. Yield was 78%; found: C, 58.28%; H, 3.78%; N, 18.13%; calcd. For $C_{38}H_{28}N_{10}O_2S_2Mn$: C, 58.83%; H, 3.64%; N, 18.06%. IR (selected bands): $\tilde{\nu}$ = CH b (oop): 700 (s) and 724 (m); CH b: 1306 (m); CCst: 1418 (m); C═N st: 1595 (m); S—CN st: 2060 (s); CH st: 3045 (w), NH st and OH st: 3390 (w) cm^{-1}.

2.1.2. Synthesis of $[Mn_2(HL)_2(SCN)_4]$ (**2**) and $[Mn_4(L)_4(SCN)_4]\cdot 2(CH_3CN)$ (**3**)

Compounds **2** and **3** were prepared using n-C_3H_7OH and CH_3CN as solvent, respectively, using the same starting materials and procedure as for the compound **1**. For **2**: yield, 60%; found: C, 51.08%; H, 2.58%; N, 17.90%; calcd. for $C_{40}H_{28}N_{12}O_2S_4Mn_2$: C, 50.74%; H, 2.98%; N, 17.75%. FT-IR (selected bands): $\tilde{\nu}$ = CH b (oop): 698 (s) and 735 (m); CH b: 1281 (m); CCst: 1474 (m); C═N st: 1590 (m); S—CN st: 2049 (s); CH st: 3050 (w), NH st and OH st: 3370 (w) cm^{-1}. For **3**: yield 86%. Found: C, 55.39%; H, 3.48%; N, 17.78%. Calculated for $C_{80}H_{58}N_{22}O_4S_4Mn_4$: C, 55.24%; H, 3.36%; N, 17.72%. FT-IR (selected bands): $\tilde{\nu}$ = CH b (oop): 698 (s) and 748 (m); CC st: 1363 (m) and 1466 (m); C═N st: 1520 (m), 1596 (m); S—CN st: 2056 (s); CH st: 3059 (w).

2.2. X-ray crystallography

Single crystals of **1**–**3** suitable for X-ray analyses were selected and used for crystallographic data collection on a Bruker AXS SMART APEX CCD diffractometer using Mo-Kα radiation (λ = 0.71073 Å) in the ω-scan mode, at room temperature for **1** and **2** and at 110(2) K for **3**. The detector frames were integrated by using the SAINT program [10] and data were corrected for absorption with SADABS program [11]. All the structures were solved by direct methods and refined by full matrix least-squares procedures using the SHELXTL [12]. All non-hydrogen atoms were refined with anisotropic displacement parameters whereas hydrogen atoms were placed at calculated positions with isotropic U values 1.2 times that of the atom to which they are bonded. In compound **1** the phenyl ring C7/C12 and the N(10)CS anion were found disordered over two positions, each at half occupancy. In **2**, one lattice acetonitrile molecule was found disordered over three positions (assigned occupancies of 0.15, 0.35, and 0.50, based on the difference Fourier map peaks). Materials for publication were prepared using WinGX [13], Cameron [14] and Diamond 3.1 [15] programs. Crystallographic data and details of refinements are given in Table 1.

2.3. Hirshfeld Surface analysis

Hirshfeld Surface (HS) analysis has become a very valuable computational method in description of crystal structures [16–20]. HS has been generated using Crystal Explorer 3.1 software [21]. Crystal structures have been imported as CIF files. Fingerprint plots have been generated using the same program.

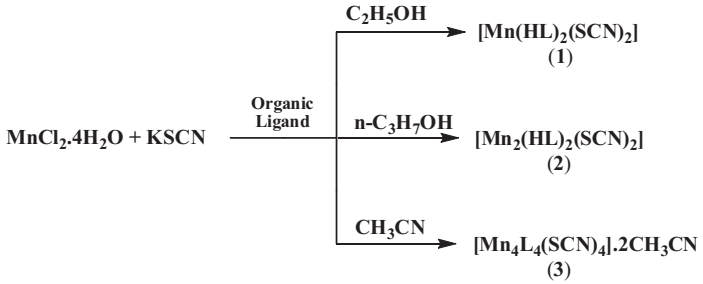

Scheme 2. Synthesis of complexes **1**–**3**.

Table 1
Crystallographic data and details of refinements for complexes **1**–**3**.

	1	**2**	**3**·2(CH_3CN)
Empirical formula	$C_{38}H_{28}MnN_{10}O_2S_2$	$C_{40}H_{28}Mn_2N_{12}O_2S_4$	$C_{80}H_{58}Mn_4N_{22}O_4S_4$
M	775.76	889.48	1739.48
Crystal system	Monoclinic	Monoclinic	Monoclinic
Space group	$P2_1/c$	$P2_1/c$	$P2_1/n$
a/Å	19.3190(4)	9.3272(3)	15.882(3)
b/Å	10.4760(7)	15.5037(5)	27.950(4)
c/Å	18.4680(10)	14.8996(7)	18.098(4)
β/°	100.113(1)	97.325(1)	100.910(9)
V/Å3	3679.6(3)	2136.99(14)	7888(2)
Z	4	2	4
Dcalc/g cm^{-3}	1.400	1.472	1.465
μ/mm^{-1}	0.522	0.837	0.797
F(0 0 0)	1596	964	3552
Theta range/°	2.22–25.16	2.20–28.26	1.57–25.44
Total data	18,580	9060	39,730
Unique data	6503	4919	14,346
R_{int}	0.1944	0.0762	0.1796
Reflections I > 2σ(I)	2454	2145	5151
Parameters	536	274	1032
Goodness-of-fit	0.913	0.996	0.943
R1 [a]	0.0647	0.0435	0.0769
wR_2 (I > 2σ(I))[a]	0.1165	0.0672	0.1332
Residuals/e $Å^{-3}$	0.360, −0.366	0.308, −0.415	0.793, −0.709

[a] $R1 = \Sigma||Fo| - |Fc||/\Sigma|Fo|$, $wR2 = [\Sigma w(Fo^2 - Fc^2)^2/\Sigma w (Fo^2)2]^{½}$.

2.4. Computational methods

The energies of all complexes included in this study were computed at the B3LYP/6-31+G** level of theory using the crystallographic geometries within the program G09 [22]. The interaction energies were computed by calculating the difference between the energies of isolated monomers and their assembly. The Bader's theory of "atoms-in-molecules" [23] has been used to characterize the interactions at the same level of theory by means of the AIMAll program [24].

3. Results and discussion

3.1. Synthesis and spectroscopic results

One-pot synthesis of a 1:1 M ratio of Mn(II) salts and HL in the adequate solvent afforded the mono-, di- and polynuclear manganese(II) compounds **1**–**3** in good yields. Their synthetic route is summarized in Scheme 2.

The new complexes are characterized by microanalytical (C, H and N), spectroscopic and other physicochemical techniques. The microanalytical data are in good conformity with the formulations of **1**–**3**. The ν_{as}(N═C═S) and ν(C—S) stretches of S-coordinated thiocyanate appear as strong bands respectively at 2111 and 765 cm^{-1}. Additionally, a band belonging to the deformation frequency δ(NCS) is found at 452 cm^{-1}. All other organic ligand vibrations are observed in the range 1600–600 cm^{-1}.

3.2. Crystal structures of *1*–*3*

An Ortep view of complex [Mn(HL)$_2$(SCN)$_2$] (**1**) is shown in Fig. 1 and relevant bond lengths and angles are listed in Table 2. The structural analysis of the complex shows the two neutral hydrazone ligands coordinated to Mn(II) in a different coordination mode, namely acting as chelating N,O through the 2-pyridine-ketone fragment and tridentate N,N,O by using the carbonyl oxygen, the imine and pyridine nitrogen atoms with formation of one and two fused five-membered chelate rings, respectively. Thus the metal exhibits a pentagonal-bipyramidal coordination geometry, where the equatorial plane is built by the O2,N8 and O1,N1,N2

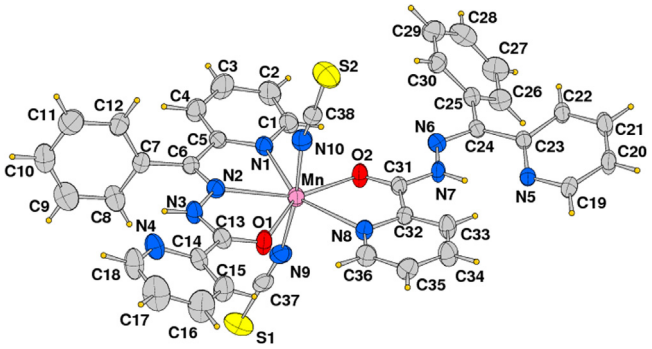

Fig. 1. ORTEP drawing (ellipsoids at 40% probability level) of complex **1**. (Thiocyanate N10 and phenyl ring C7-12 are disordered over two positions, only one group is depicted.)

Table 2
Coordination bond distances (Å) and angles (°) of complex **1**.

Mn—N(1)	2.398(4)	Mn—O(2)	2.231(4)
Mn—N(2)	2.328(5)	Mn—N(9)	2.140(5)
Mn—O(1)	2.382(4)	Mn—N(10)	2.100(19)
Mn—N(8)	2.419(5)	Mn—N(10b)*	2.19(2)
N(1)—Mn—N(2)	67.14(16)	O(1)—Mn—N(8)	77.38(15)
N(1)—Mn—O(1)	134.48(16)	O(1)—Mn—O(2)	146.91(15)
N(1)—Mn—N(8)	148.05(16)	O(1)—Mn—N(9)	86.97(18)
N(1)—Mn—O(2)	78.60(15)	O(1)—Mn—N(10)	87(4)
N(1)—Mn—N(9)	88.34(17)	N(8)—Mn—O(2)	69.62(15)
N(1)—Mn—N(10)	92(2)	N(8)—Mn—N(9)	97.28(17)
N(2)—Mn—O(1)	67.36(15)	N(8)—Mn—N(10)	87(2)
N(2)—Mn—N(8)	144.44(16)	O(2)—Mn—N(9)	94.75(18)
N(2)—Mn—O(2)	145.72(16)	O(2)—Mn—N(10)	93(4)
N(2)—Mn—N(9)	85.63(18)	N(9)—Mn—N(10)	172(4)
N(2)—Mn—N(10)	87(3)		

* N(10b) represents the coordinated atom of the disordered NCS ligand (bond angles pertaining to this atom not shown).

donors of the HL ligands, while the axial positions are occupied by the linearly coordinated NCS anions bound through the nitrogen donor. The Mn—O and Mn—N bond lengths involving the hydrazine ligands fall in the range 2.231(4)–2.419(5) Å, close similar to those measured in the complex with the heptacoordinated 2,6-diacetylpyridine bis(hydrazone) ligand [25], but significantly longer than those detected in the [Mn(L1)$_2$] [26] where L1 ligands, N,N,O meridionally coordinated, differs from HL for an uncoordinated pyridine replacing the phenyl group.

On the other hand the equatorial coordination distance values are significantly longer than those of the axial Mn-NCS bond lengths of 2.140(5) and 2.100(19) Å. With exception of the phenyl ring, the tricoordinated ligand has almost coplanar atoms within ±0.2 Å, while in the other ligand the pyridine forms a dihedral angle of 20.8° with the pyridin-2-carbohydrazide moiety. In both ligands intramolecular H bonds that reinforce the overall structure occur between the NH fragments and uncoordinated py nitrogen atoms [N···N distance of 2.649(7) and 2.587(6) Å, *N*—H···N angle of 103 and 137°, respectively]

The crystal packing does not show significant π-π interactions as it would be expected and the most relevant one being that between the disordered phenyl (see experimental section) C7b/C12b with N4 py of a symmetry related complex (distance between ring centroids of 3.947(5) Å. The complex [Mn(L2)$_2$(N$_3$)$_2$] [27], where L2 = *N*′-((pyridin-2-yl)methylene)benzohydrazide, N_3 = azide, reported a few years ago shows a similar structure indicating that the presence of pseudohalide anions leads for steric hindrance to a different coordination mode of the two hydrazone ligands in case of mononuclear complex. Finally, the pseudohalide also acts as H-bond acceptor that is further described below in the DFT study (Fig. 2).

In complex **2** a pair of adjacent [Mn(HL)(SCN)] units is linked by two bridging μ-(1,1)-NCS ligands, resulting in a dinuclear complex unit located about a crystallographic inversion center. Each Mn atom is coordinated by one O and two N atoms of the tridentate ligand and three thiocyanate anions, forming a distorted MnN_5O octahedron. The Mn—N and Mn—O coordination distances (Table 3) involving the tridentate ligand moiety are ca. 0.1 Å shorter than those measured in **1**. The bridging NCS anions exhibit unsymmetrical coordination showing significantly different Mn—N6 distances, of 2.159(3) and 2.441(3) Å, with a Mn—N6—Mn1′ angle of 100.16(10)°. Data of Table 3 evidence the distortions of bond angles from ideal values due to the requirement to form the chelating N1—Mn—N2 and N2—Mn—O1 angles of 70.38(9) and 71.12(8)°, respectively. The intermetallic Mn—Mn distance in the complex is of 3.532 Å. The molecular conformation is stabilized by intramolecular N3—H···N4 hydrogen bonds (N···N = 2.644(4) Å, NHN angle = 105(2)°). In the crystal, the shorter π–π stacking interaction (centroid–centroid distance = 3.9680(18) Å) occurs between C7/C12 phenyl rings of symmetry related complexes. The complex has a structure similar to that of $[Cd_2(HL)_2Cl_4]$ [28], where the chlorides replace the thiocyanate anions.

The crystal structure of **3** is shown in Fig. 3, while a selection of bond lengths and angles relevant to the coordination spheres are given in Table 4. The asymmetric unit consists of a tetranuclear Mn(II) complex with metals connected by four deprotonated L ligands. The Mn(II) ions exhibit different coordination environments. In fact the Mn2 and Mn4 are coordinated by two oxygen and four nitrogen atoms from two different L ligands, while Mn1 and Mn3 ions are coordinated by two oxygen and two nitrogen atoms from two L ligands completing their coordination sphere by two NCS ligands. The complex structure exhibits a pseudo twofold symmetry with axis passing in the center of the almost coplanar (±0.03 Å) Mn_4 entity. This architecture is realized by four distorted MnN_4O_2 octahedral units built by four N,N,O,N tetradentate ligands where each oxygen atom bridges two metal ions with Mn—O distances in the range 2.141(6)–2.237(6) Å and Mn—O—Mn angles in between 126.7(3)–127.6(3)°. The Mn—N(py) bond lengths (range 2.236(6)–2.318(7) Å) are longer than the Mn—N (imine) bond values (2.185(7)–2.214(7) Å), and the Mn—NCS are the shortest, 2.129(8)–2.145(7) Å.

The metal rhomboid arrangement has edges (Mn—Mn distances) in the range 3.841–3.940 Å and angles of ca 73° and 107° at Mn1/3 and Mn2/4, respectively. The recently reported complex $[Mn_4(L3)_4(N3)_4]$ [29], where ligand L3 differs from L for a methyl replacing the phenyl group, has a comparable configurational arrangement. In the same paper a structural isomer of complex **3** has been described having a SCN anion bound at each

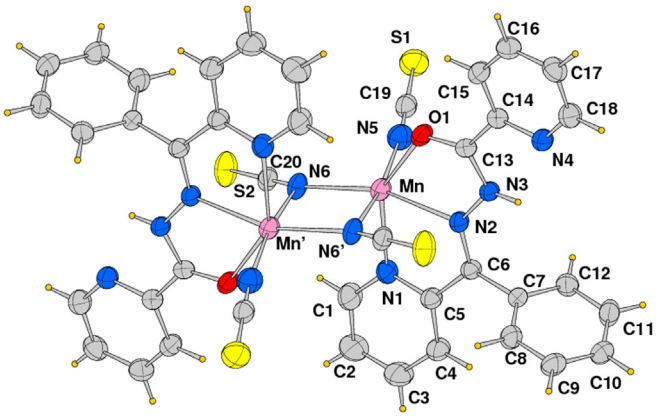

Fig. 2. ORTEP drawing (ellipsoids at 40% probability level) of the centrosymmetric complex **2** with labelling scheme of the crystallographic independent unit.

Table 3
Coordination bond distances (Å) and angles (°) of complex **2**.

Mn—N(1)	2.272(3)	Mn—N(6)	2.159(3)
Mn—N(2)	2.226(2)	Mn—O(1)	2.253(2)
Mn—N(5)	2.104(3)	Mn—N(6′)	2.441(3)
N(1)—Mn—N(2)	70.38(9)	N(5)—Mn—O(1)	87.41(10)
N(1)—Mn—N(5)	107.75(10)	N(6)—Mn—O(1)	120.84(9)
N(1)—Mn—N(6)	93.91(10)	N(1)—Mn—N(6′)	85.74(9)
N(1)—Mn—O(1)	140.47(8)	N(2)—Mn—N(6′)	85.78(8)
N(2)—Mn—N(5)	100.04(10)	N(5)—Mn—N(6′)	166.42(10)
N(2)—Mn—N(6)	159.51(10)	N(6)—Mn—N(6′)	79.84(10)
N(2)—Mn—O(1)	71.12(8)	O(1)—Mn—N(6′)	82.86(8)
N(5)—Mn—N(6)	97.23(10)		

Primed atoms at −x + 1, −y, −z.

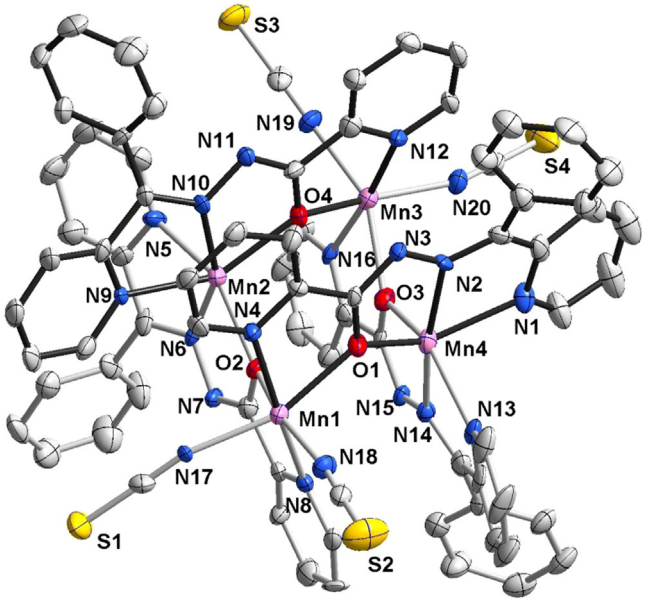

Fig. 3. ORTEP drawing (ellipsoids at 50% probability level) of complex **3** (labels of C atoms not shown for clarity).

metal resulting in a S_4 symmetry. Fig. 4 reports a scheme of the structure the two isomers showing the different arrangement of ligands that in each case leave four vacant sites at metals occupied by the SCN anions. The crystal packing of complex **3** shows voids in the solid state occupied by solvent molecules (Fig. 5). It is worth of note that the formation of tetranuclear complexes represents a common feature with these kind of ligands as represented by the examples reported with Mn and Cu ions where the metals complete their coordination sphere with aqua ligands or coordinating anions (CF_3SO_3 or azide) [3].

3.3. Hirshfeld Surface analysis

Hirshfeld Surface of compound **1** mapped with d_{norm} function is covered profusely with red areas of different sizes (Fig. 6). A large part of them – ten – corresponds to five short H···H contacts. (H17···H9, H10···H20, H12···H9, H12···H8, H16···H12B). This, as well as a big percentage of Hirshfeld Surface contributing to H···H contacts (32.5%; based on decomposed fingerprint plot, Fig. 7) indicates van der Waals and possibly C—H···π interactions. Presence and significance of the latter is also visible in shape of eight red spots (two big and six smaller ones) corresponding to four C—H···C contacts (C21—H21···C38, C34—H34···C28, C18—H18···C38, C30—H30···C19). H···C contacts contribute to 29.9% of the surface (Fig. 7b). Importance of van der Waals and

Table 4
Coordination bond distances (Å) and angles (°) of complex **3**.

Mn(1)—N(4)	2.236(6)	Mn(3)—N(12)	2.260(7)
Mn(1)—N(8)	2.240(7)	Mn(3)—N(16)	2.271(7)
Mn(1)—N(17)	2.145(7)	Mn(3)—N(19)	2.143(7)
Mn(1)—N(18)	2.129(8)	Mn(3)—N(20)	2.145(8)
Mn(1)—O(1)	2.214(6)	Mn(3)—O(3)	2.208(6)
Mn(1)—O(2)	2.237(6)	Mn(3)—O(4)	2.235(6)
Mn(2)—N(5)	2.318(7)	Mn(4)—N(1)	2.262(8)
Mn(2)—N(9)	2.313(7)	Mn(4)—N(13)	2.277(7)
Mn(2)—N(6)	2.185(7)	Mn(4)—N(2)	2.214(7)
Mn(2)—N(10)	2.203(7)	Mn(4)—N(14)	2.204(7)
Mn(2)—O(2)	2.154(5)	Mn(4)—O(1)	2.141(6)
Mn(2)—O(4)	2.153(5)	Mn(4)—O(3)	2.183(6)
N(18)—Mn(1)—N(17)	101.7(3)	N(19)—Mn(3)—N(20)	103.1(3)
N(18)—Mn(1)—O(1)	94.3(2)	N(19)—Mn(3)—O(3)	153.1(2)
N(17)—Mn(1)—O(1)	160.7(2)	N(20)—Mn(3)—O(3)	95.9(2)
N(18)—Mn(1)—N(4)	96.6(3)	N(19)—Mn(3)—O(4)	89.4(3)
N(17)—Mn(1)—N(4)	93.7(2)	N(20)—Mn(3)—O(4)	158.3(3)
O(1)—Mn(1)—N(4)	73.5(2)	O(3)—Mn(3)—O(4)	79.1(2)
N(18)—Mn(1)—O(2)	163.1(3)	N(19)—Mn(3)—N(12)	87.6(3)
N(17)—Mn(1)—O(2)	88.8(2)	N(20)—Mn(3)—N(12)	90.2(3)
O(1)—Mn(1)—O(2)	78.5(2)	O(3)—Mn(3)—N(12)	111.4(2)
N(4)—Mn(1)—O(2)	95.9(2)	O(4)—Mn(3)—N(12)	72.3(2)
N(18)—Mn(1)—N(8)	94.0(3)	N(19)—Mn(3)—N(16)	87.6(3)
N(17)—Mn(1)—N(8)	88.5(2)	N(20)—Mn(3)—N(16)	92.2(3)
O(1)—Mn(1)—N(8)	101.2(2)	O(3)—Mn(3)—N(16)	72.6(2)
N(4)—Mn(1)—N(8)	168.5(3)	O(4)—Mn(3)—N(16)	106.2(2)
O(2)—Mn(1)—N(8)	72.9(2)	N(12)—Mn(3)—N(16)	175.0(2)
O(4)—Mn(2)—O(2)	103.79(19)	O(1)—Mn(4)—O(3)	108.9(2)
O(4)—Mn(2)—N(6)	123.2(2)	O(1)—Mn(4)—N(14)	119.3(2)
O(2)—Mn(2)—N(6)	71.3(2)	O(3)—Mn(4)—N(14)	71.0(2)
O(4)—Mn(2)—N(10)	71.8(2)	O(1)—Mn(4)—N(2)	71.2(2)
O(2)—Mn(2)—N(10)	125.7(2)	O(3)—Mn(4)—N(2)	106.3(2)
N(6)—Mn(2)—N(10)	156.7(2)	N(14)—Mn(4)—N(2)	169.5(3)
O(4)—Mn(2)—N(9)	142.6(2)	O(1)—Mn(4)—N(1)	140.1(3)
O(2)—Mn(2)—N(9)	96.0(2)	O(3)—Mn(4)—N(1)	93.1(2)
N(6)—Mn(2)—N(9)	93.0(2)	N(14)—Mn(4)—N(1)	99.0(3)
N(10)—Mn(2)—N(9)	70.8(2)	N(2)—Mn(4)—N(1)	70.8(3)
O(4)—Mn(2)—N(5)	98.1(2)	O(1)—Mn(4)—N(13)	90.7(2)
O(2)—Mn(2)—N(5)	142.5(2)	O(3)—Mn(4)—N(13)	141.8(3)
N(6)—Mn(2)—N(5)	71.3(3)	N(14)—Mn(4)—N(13)	70.8(3)
N(10)—Mn(2)—N(5)	89.9(3)	N(2)—Mn(4)—N(13)	111.1(3)
N(9)—Mn(2)—N(5)	84.0(2)	N(1)—Mn(4)—N(13)	91.7(3)

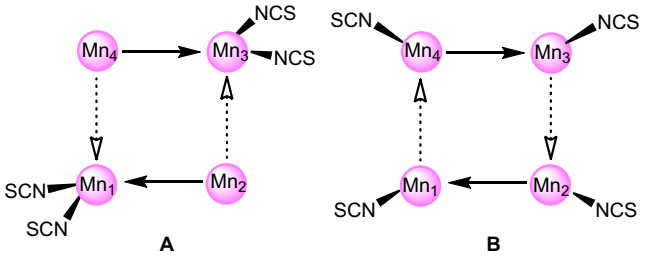

Fig. 4. Scheme of the different isomers observed for $[Mn_4(L)_4(SCN)_4]$: (A) this work; (B) from Ref. [29] (The arrow head indicates the 2-pyridine-ketone N,O-chelating moiety, the plain and dashed arrows are above and below the Mn_4 plane, respectively).

stacking interactions is further highlighted by lack of strong conventional hydrogen bonds. All contacts involving electronegative atoms (N, S) are of weak C — H···X type (C28—H28···N6, C4—H4···N4, C19—H19···N9, C8B—H8B···S2 and C11B—H11B···S1), which are manifested by eight red areas on the surface. When the surface is mapped with shape index function 'bow-tie' patterns are visible (Fig. 6). They correspond to π···π stacking interactions.

On the Hirshfeld Surface of **2** mapped with d_{norm} function one can notice sixteen red areas. Due to symmetry of the molecule they correspond to four individual weak interactions. Three of them are

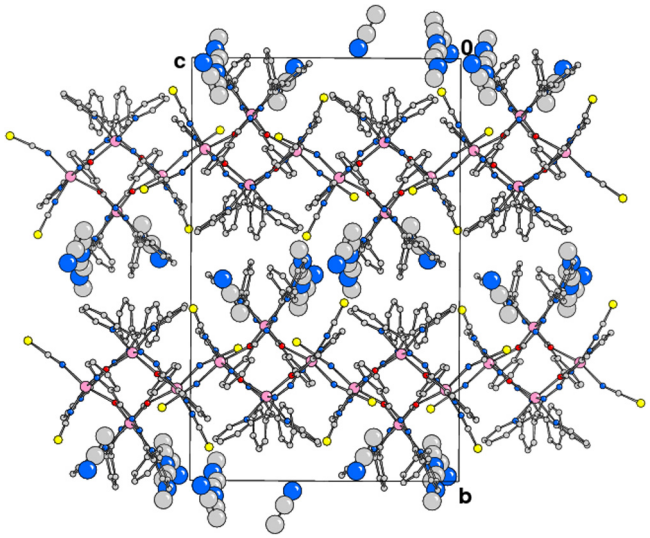

Fig. 5. View of crystal packing down axis *a* of complex **3**. Big spheres indicate the disordered acetonitrile lattice molecules.

C—H···C interactions. One of those is consistent with a C—H···π interaction (C8—H8···C17; big red areas), while the other two are formed between two different pyridyl rings of one complex molecule and one of the thiocyanate ions of the adjacent molecule (C16—H16···C19, C2—H2···C19). One last short contact is formed between a hydrogen and a nitrogen atom, corresponding to a C—H···N weak interaction (C11—H11···N5). Like in compound **1** most of the surface comprises H···H and H···C contacts (23.1% and 25.4% respectively), which underlines the importance of van der Waals forces and C—H···π interactions. Stacking interactions between aromatic rings also play a major role and can be easily localized when the surface is mapped with shape index function (Fig. 8). Analysis of decomposed fingerprint plots (Fig. 7) indicates that H···S contacts make up a huge part of the surface (25.8%), however no close contacts of this type are present.

Hirshfeld surface of compound **3** is dotted with a large amount of red areas (Fig. 9). One big red dot stands out particularly. It corresponds to a short H···C contact between the coordination molecule and a disordered solvent molecule (C20—H20···C84). Additionally, there are a total of fourteen red areas indicative of numerous other C···H contacts. Two bigger ones correspond to two interactions between one of the aromatic ring of the complex molecule and a disordered lattice solvent molecule (C56—H56···C84 and C55—H55···C84). Smaller red spots are present due to existence of several other C—H···C interactions. These occur either between pyridyl rings of one complex compound and thiocyanate ions of the other (C52—H52···C74, C53—H53···C73, C16—H16···C76 and C64—H64···C73) or between pyridyl rings and lattice acetonitrile molecules (C80—H80C···C48 and C47—H47···C77). Moreover, there are a large number of red spots – eleven – corresponding to six C—H···S interactions (C39—H39···S1, C34—H34···S4, C4—H4···S1, C78—H78···S4, C22—H22···S3 and C52—H52···S2). Since most of nitrogen atoms of the complex molecule are involved in coordination bonds and are positioned away from the HS, the only H···N contacts that are short enough to be shown on the surface are those involving lattice solvent molecules (C20—H20···N23, C65—H65···N21 and C3—H3···N21). Lastly there is one small red spot which corresponds to a short H···H contact (H12···H44). When the surface is mapped with shape index function 'bow-tie' patterns can be seen (Fig. 8). These are consistent with presence of π···π stacking interactions. Like in the previous compounds H···H (37.3%), H···C

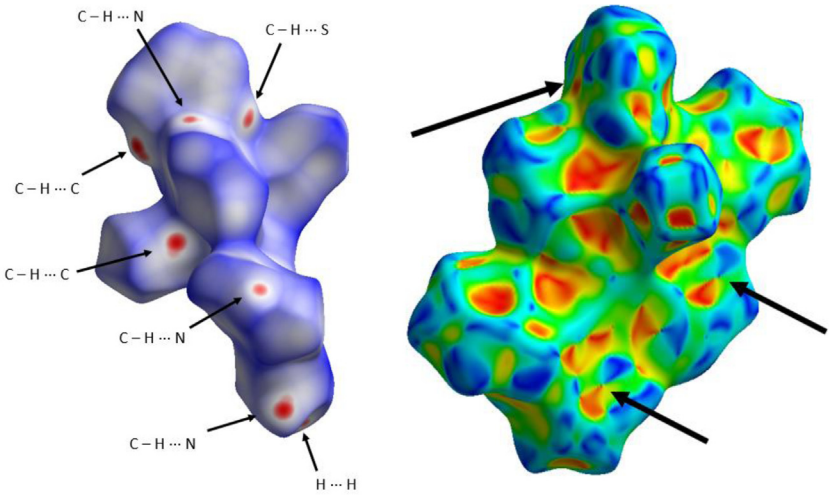

Fig. 6. Left: Hirshfeld surface of **1** mapped with d_{norm} function. Right Hirshfeld surface of **1** mapped with shape index function. Arrows indicate 'bow-tie' patterns.

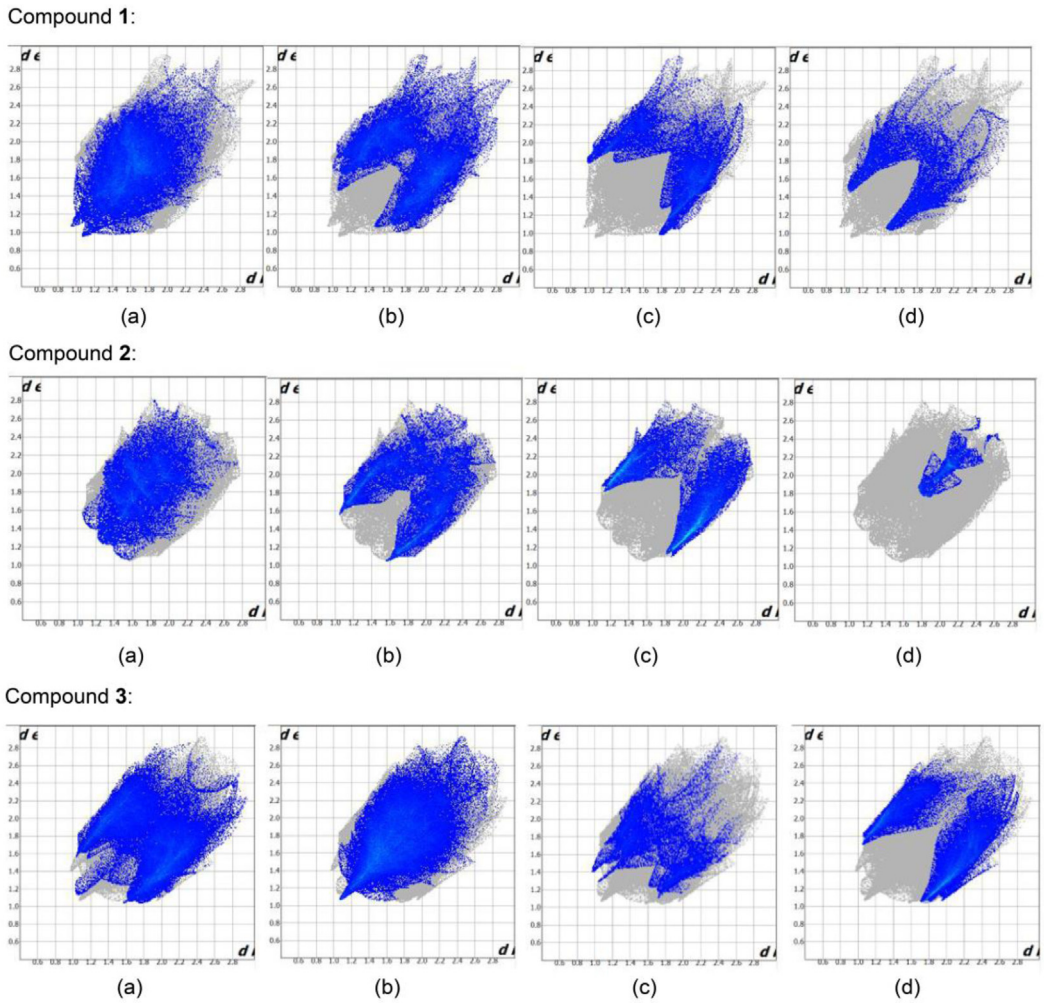

Fig. 7. Decomposed fingerprint plots of **1**–**3**; 1: a) H···H; b) H···C; c) H···N; d) H···S. 2: a) H···H; b) H···C; c) H···S; d) C···C. 3: a) H···C; b) H···H; c) H···N; d) H···S.

(26.4%) and H···S (19.2%) contacts make up most of the Hirshfeld surface (see Fig 7). Decomposed fingerprint plots show significant asymmetry due to the fact that some of the interactions involve solvent molecules situated outside of the surface.

3.4. DFT calculations

The theoretical study is devoted to analyse some "unconventional" noncovalent interactions that participate in the crystal

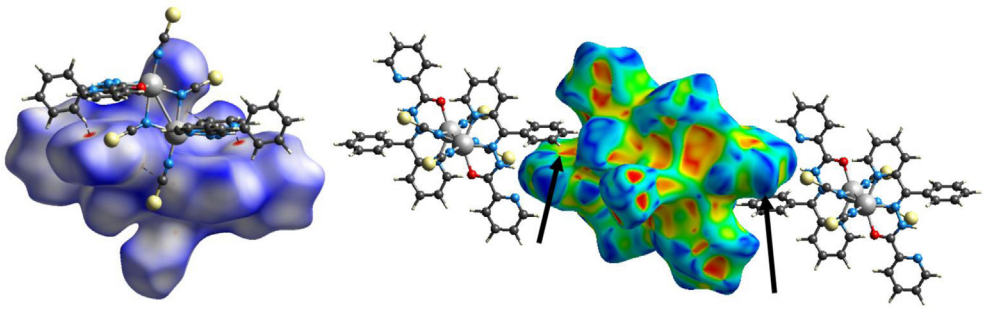

Fig. 8. Left: Hirshfeld surface of **2** mapped with d_{norm} function. Weak C — H···X (X = C, N) marked as dashed lines. Right: Hirshfeld surface of **2** mapped with shape index function. Arrows indicate 'bow-tie' patterns.

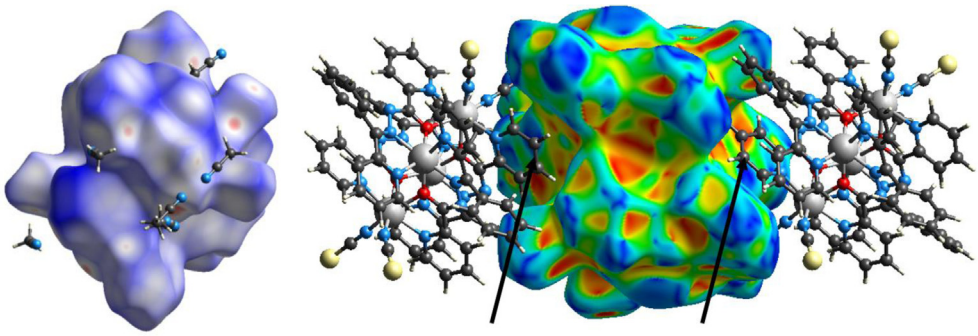

Fig. 9. Left: Hirshfeld surface of **3** mapped with d_{norm} function. Right: Hirshfeld surface of **3** mapped with shape index function. Arrows indicate 'bow-tie' patterns.

packing of compounds **1**–**3**, in particular the C—H···π interactions. The importance of the C—H···π interaction in the solid state where the π-system is an aromatic ring has been studied in depth by Nishio [30]. However, studies on C—H···π interactions where the π-system belongs to a coordinated pseudohalide ligands are scarcely found in the literature.

As a first approximation to rationalize the unconventional C—H···π ·interactions involving the NCS– ligand observed in the solid state of compounds **1**–**3** (*vide infra*), we have computed the Molecular Electrostatic Potential (MEP) surface of **1** as exemplifying compound, which is shown in Fig. 10. As expected, in both complexes the most positive regions (blue surface) correspond to the aromatic H atoms of HL. The most negative region (red surface) corresponds to the pseudohalide ligands (N and S atoms). Interestingly, the NCS ligand is a better H-bond acceptor via the π-system (−55 and −49 kcal/mol at the negative belts of the S and N atoms) than via the σ-system (−33 kcal/mol at the extension of the NCS σ-bonds).

In Fig. 11a we show a partial view of the crystal packing of compound **1** to highlight the crucial role of several C—H···π interactions. Basically, self-assembled dimers are formed by a combination of C—H···π(NCS) and other long range dispersion. Each dimer further interacts with the adjacent ones by means of conventional C—H···π(arene) interactions. We have examined first the interaction energy of the self-assembled dimer where two symmetry related C—H···π(NCS) interactions are established (see Fig. 11b) in addition of other long range van der Waals interactions. This combination of noncovalent forces explains the large interaction energy computed for this dimer (ΔE_1 = −20.1 kcal/mol) and agrees with the excellent H-bond acceptor ability of the pseudohalide ligand anticipated in the MEP analysis (see Fig. 9). In an effort to evaluate the contribution of the C—H···π(NCS) interactions, we have computed an additional theoretical model where the pyridine rings have been eliminated (replaced by H atoms, see small arrows in Fig. 11c). The interaction energy of this

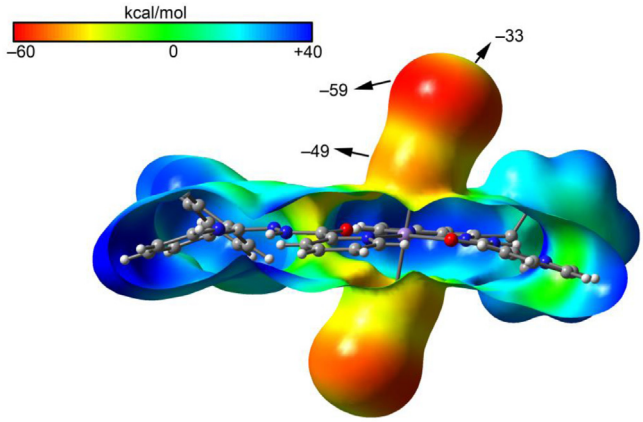

Fig. 10. MEP surface of compound **1**. Energies at selected points of the surface are given in kcal/mol.

hypothetical dimer (Fig. 11c) is ΔE_2 = −8.9 kcal/mol that can be attributed to the contribution of the additional long range van der Waals interactions and the difference (ΔE_1–ΔE_2 = −11.2 kcal/mol) is a rough estimation of both symmetrically equivalent C—H···π interactions. This energetic study confirms the importance of these interactions in the formation of the dimer. Furthermore, we have used the Bader's theory of "atoms in molecules" (AIM) to characterize the noncovalent bonds described above for complex **1** as a model system. The AIM analysis has been used to characterize a variety of interactions, included those studied herein [31]. A bond critical point (CP) and a bond path connecting two atoms is an unambiguous evidence of interaction [23]. The AIM distribution of critical points and bond paths computed for the self-assembled dimer of compound **1** is shown in Fig. 11c. For the sake of clarity, only those CPs and bond paths that connect the H

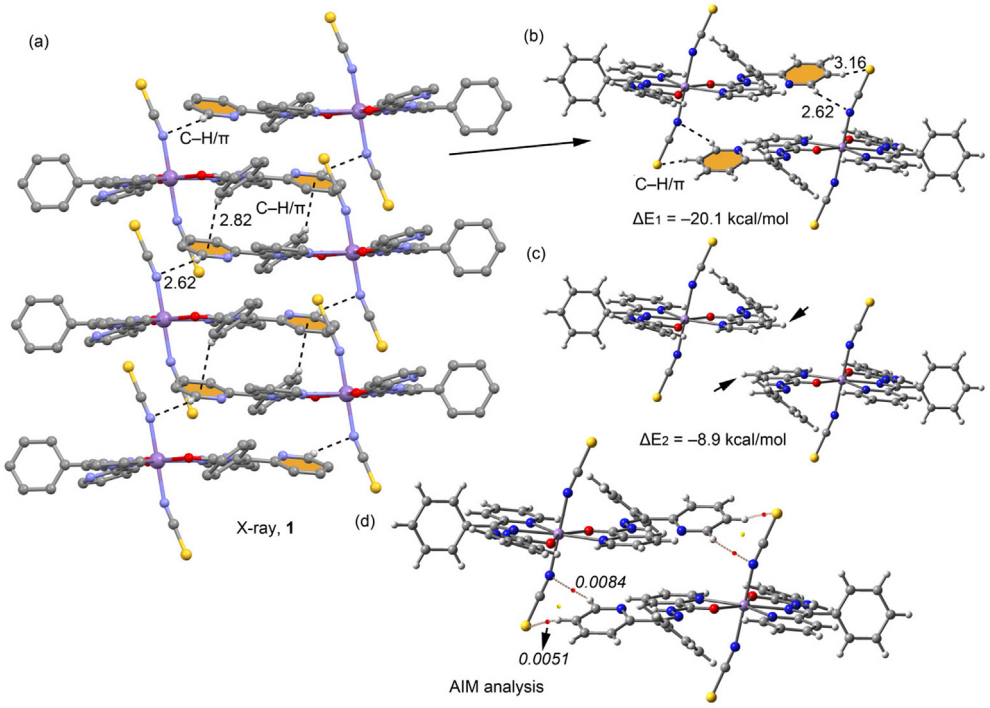

Fig. 11. (a) Detail of the crystal packing of **1**, H-atoms omitted for clarity. (b,c) Theoretical models used to evaluate the π–π, H-bonding, lp–π and C—H···π interactions. Distances in Å. (d) Distribution of bond and ring critical points (red and yellow spheres, respectively) and bond paths is represented for the dimer of compound **1**. The values of ρ(r) at the bond CPs are given in a.u. (values in italics). (For interpretation of the references to colour in this figure legend, the reader is referred to the web version of this article.)

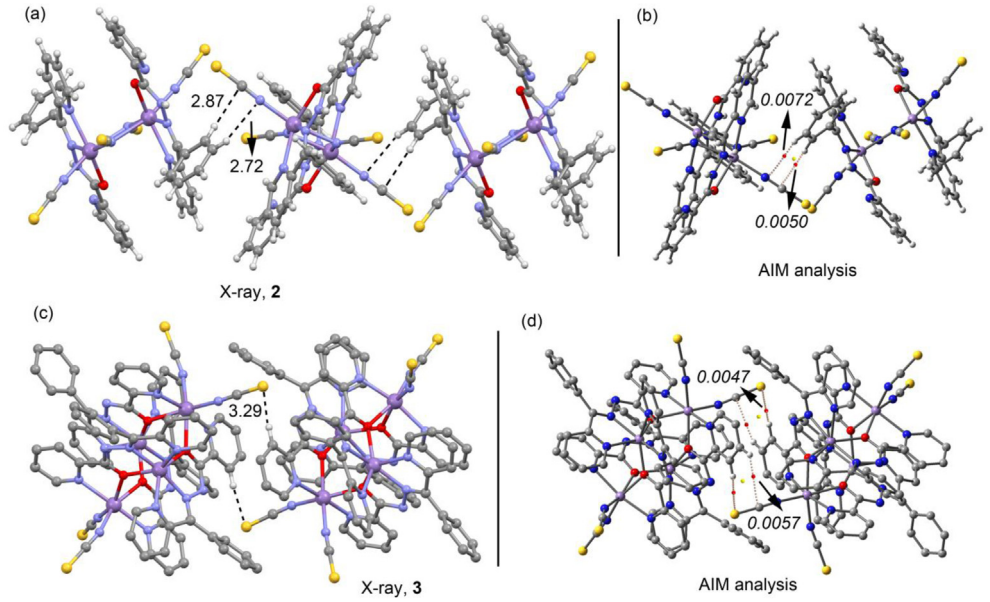

Fig. 12. (a, c) X-ray fragments of **2** and **3**, several H-atoms omitted for clarity. Distances in Å. (b, d) Distribution of bond and ring critical points (red and yellow spheres, respectively) and bond paths is represented for the dimer of compounds **2** and **3**. The values of ρ(r) at the bond CPs are given in a.u. (values in italics). (For interpretation of the references to colour in this figure legend, the reader is referred to the web version of this article.)

atoms of pyridine to the NCS ligands are shown. The distribution reveals that each C—H···π interaction is characterized by two bond CPs (red spheres) and bond paths connecting the N and S atoms of the pseudohalide with two H atoms of pyridine (see Fig. 11c). The interaction is further characterized by a ring CP (yellow sphere) as a consequence of the formation of a supramolecular ring.

Finally, in Fig. 12 we represent two fragments of the X-ray solid state structures of compounds **2** and **3** where C—H···π(NCS) interactions are highlighted to further demonstrate the ability of the π-system of the Mn—N=C=S moiety to participate in H-bonds. In compound **2** an infinite 1D chain is formed in the solid state stabilized, among others, by these interactions (see Fig. 12a). We have

characterized them using the AIM analysis of critical points that reveals the appearance of two bond CPs (red spheres) and bond paths connecting the N and C atoms of the pseudohalide with two H atoms of a phenyl ring of the ligand (see Fig. 12b). The interaction is further characterized by a ring CP (yellow sphere) as a consequence of the formation of a supramolecular ring. In Fig. 12c we represent a dimer observed in the solid state of compound **3** where C—H···π(NCS) contacts in addition to other long range dispersion interactions are established. The AIM analysis also shows two bond CPs (red spheres) and bond paths connecting the N and C atoms of the pseudohalide with two H atoms of a pyridine moiety of the ligand (see Fig. 12d). The interaction is further characterized by a ring CP (yellow sphere). The values of charge density at the bond CPs are also indicated in Fig. 12b,c that are comparable to those previously observed in the dimer of compound **1** (see Fig. 11d) and confirm the existence of the unconventional C—H···π interaction.

4. Concluding remarks

In the present study we have synthesized and X-ray characterized three Mn(II) derivatives with 2-benzoylpyridyl-(2-picolyl)-hydrazone ligand (HL) and SCN anions having different nuclearity. The complexes have been obtained by using in the synthesis different solvent medium that is crucial to get the different manganese derivatives. A different coordination mode of the ligand is observed in each complex, showing significant versatility due to the diverse donor sites. We have described the importance of unconventional C—H···π(NCS) interactions in the solid state of all compounds. The energetic feature of this interaction has been studied by means of DFT calculations in compound **1** and characterized using the Bader's theory of atoms in molecules in all compounds. Finally, the interactions have been also described using Hirshfeld surface analysis that further confirms the importance of the C—H···π (NCS) interactions.

Acknowledgements

We are grateful to the University of Maragheh for the financial support of this research. A.F. thanks MINECO (Spain) for financial support (projects CTQ2014-57393-C2-1-P and CONSOLIDER-Ingenio 2010 project CSD2010-0065).

Appendix A. Supplementary data

CCDC 1499457–1499459 contain the supplementary crystallographic data for **1**–**3**. These data can be obtained free of charge via http://www.ccdc.cam.ac.uk/conts/retrieving.html, or from the Cambridge Crystallographic Data Centre, 12, Union Road, Cambridge CB2 1EZ, UK; Fax: (+44) 1223-336-033; or e-mail: deposit@ccdc.cam.ac.uk. Supplementary data associated with this article can be found, in the online version, at http://dx.doi.org/10.1016/j.ica.2016.10.028.

References

[1] (a) X. Yang, D. Lam, C. Chan, J.M. Stanley, R.A. Jones, B.J. Holliday, W.K. Wong, Dalton Trans. 40 (2011) 9795;
(b) J. Sanmartín, A.M. García-Deibe, M.R. Bermejo, F. Novio, D. Navarro, M. Fondo, Eur. J. Inorg. Chem. (2003) 3905;
(c) J.C. Jiang, Z.L. Chu, W. Huang, G. Wang, X.Z. You, Inorg. Chem. 49 (2010) 5897.
[2] (a) M.R. Maurya, N. Chaudhary, F. Avecilla, P. Adão, J. Costa Pessoa, Dalton Trans. 44 (2015) 1211–1232;
(b) N.A. Mangalam, S. Sivakumar, S.R. Sheeja, M.R.P. Kurup, E.R.T. Tiekink, Inorg. Chim. Acta 362 (2009) 4191–4197;
(c) R. Bikas, P. Aleshkevych, H. Hosseini-Monfared, J. Sanchiz, R. Szymczak, Dalton Trans. 44 (2015) 1782–1789.
[3] (a) L.N. Dawe, T.S.M. Abedin, T.L. Kelly, L.K. Thompson, D.O. Miller, C. Liang Zhao, M.A. Wilson, J.A.K.Howard. Leech, J. Mater. Chem. 16 (2006) 2645–2659;
(b) H. Grove, T.L. Kelly, L.K. Thompson, Inorg. Chem. 43 (2004) 4278.
[4] S.S. Tandon, L.N. Dawe, V.A. Milway, J.L. Collins, L.K. Thompson, Dalton Trans. (2007) 1948–1953.
[5] I.S. Lee, D. MokShin, Y.K. Chung, CrystEngComm 11 (2009) 997–1000.
[6] (a) M.A. Withersby, A.J. Blake, N.R. Champness, P.A. Cooke, P. Hubberstey, W.-S. Li, M. Schröder, Inorg. Chem. 38 (1999) 2259–2266;
(b) S. Lopez, S.W. Keller, Inorg. Chem. 38 (1999) 1883–1888;
(c) T.L. Hennigar, D.C. MacQuarrie, P. Losier, R.D. Rogers, M. Zaworotko, Angew. Chem., Int. Ed. Engl. 36 (1997) 972–973;
(d) H. Yang, F. Cao, D. Li, S. Zeng, Y. Song, J. Dou, Dalton Trans. 44 (2015) 6620–6629.
[7] A. Hazari, L.K. Das, A. Bauzá, A. Frontera, A. Ghosh, Dalton Trans. 43 (2014) 8007–8015.
[8] P. Chakraborty, S. Purkait, S. Mondal, A. Bauzá, A. Frontera, C. Massera, D. Das, CrystEngComm 17 (2015) 4680–4690.
[9] F.M. Tabellion, S.R. Seidel, A.M. Arif, P.J. Stang, J. Am. Chem. Soc. 123 (2001) (1990) 11982–11990.
[10] SAINT Plus, Data Reduction and Correction Program, v. 6.01, Bruker AXS, Madison, Wisconsin, USA, 1998.
[11] SADABS v. 2.01, Bruker/Siemens Area Detector Absorption Correction Program, Bruker AXS, Madison, Wisconsin, USA, 1998.
[12] G.M. Sheldrick, Acta Crystallogr. A 64 (2008) 112.
[13] L.J. Farrugia, J. Appl. Crystallogr. 45 (2012) 849–854.
[14] D.M. Watkin, L. Pearce, C.K. Prout, Chemical Crystallography Laboratory, University of Oxford, 1993.
[15] K. Brandenburg, DIAMOND, Crystal Impact GbR, Bonn, Germany, 1999.
[16] M.J. Białek, J.K. Zareba, J. Janczak, J. Zon, Cryst. Growth Des. 13 (2013) 4039.
[17] J.K. Zareba, M.J. Białek, J. Janczak, J. Zon, A. Dobosz, Cryst. Growth Des. 14 (2014) 6143.
[18] J.J. McKinnon, M.A. Spackman, A.S. Mitchell, Acta Crystallogr. B 60 (2004) 627.
[19] M.A. Spackman, J.J. McKinnon, CrystEngComm 4 (2002) 378.
[20] J.J. McKinnon, D. Jayatilaka, M.A. Spackman, Chem. Commun. (2007) 3814.
[21] S.K. Wolff, D.J. Grimwood, J.J. McKinnon, M.J. Turner, D. Jayatilaka, M.A. Spackman, Crystal Explorer, Ver. 3.1, University of Western Australia, Perth, Australia, 2013.
[22] M.J. Frisch, G.W. Trucks, H.B. Schlegel, G.E. Scuseria, M.A. Robb, J.R. Cheeseman, G. Scalmani, V. Barone, B. Mennucci, G.A. Petersson, H. Nakatsuji, M. Caricato, X. Li, H.P. Hratchian, A.F. Izmaylov, J. Bloino, G. Zheng, J.L. Sonnenberg, M. Hada, M. Ehara, K. Toyota, R. Fukuda, J. Hasegawa, M. Ishida, T. Nakajima, Y. Honda, O. Kitao, H. Nakai, T. Vreven, J.A. Montgomery Jr., J.E. Peralta, F. Ogliaro, M. Bearpark, J.J. Heyd, E. Brothers, K.N. Kudin, V.N. Staroverov, R. Kobayashi, J. Normand, K. Raghavachari, A. Rendell, J.C. Burant, S.S. Iyengar, J. Tomasi, M. Cossi, N. Rega, J.M. Millam, M. Klene, J.E. Knox, J.B. Cross, V. Bakken, C. Adamo, J. Jaramillo, R. Gomperts, R.E. Stratmann, O. Yazyev, A.J. Austin, R. Cammi, C. Pomelli, J.W. Ochterski, R.L. Martin, K. Morokuma, V.G. Zakrzewski, G.A. Voth, P. Salvador, J.J. Dannenberg, S. Dapprich, A.D. Daniels, Ö. Farkas, J.B. Foresman, J.V. Ortiz, J. Cioslowski, D.J. Fox, Gaussian 09, Revision C.01, Gaussian Inc, Wallingford CT, 2009.
[23] R.F.W. Bader, Atoms in Molecules – A Quantum Theory, Oxford University Press, Oxford, U.K., 1990.
[24] Todd A. Keith, AIMAll (Version 13.05.06), TK Gristmill Software, Overland Park KS, USA, 2013.
[25] L.S. Vojinovic-Ješić, V.I. Češljević, G.A. Bogdanović, V.M. Leovac, K.M. Szecsenyi, V. Divjakovic, M.D. Joksović, Inorg. Chem. Commun. 13 (2010) 1085–1088.
[26] S. Banerjee, A. Ray, S. Sen, S. Mitra, D.L. Hughes, R.J. Butcher, S.R. Batten, D.R. Turner, Inorg. Chim. Acta 361 (2008) 2692–2700.
[27] N.A. Mangalam, S.R. Sheeja, M.R.P. Kurup, Polyhedron 29 (2010) 3318–3323.
[28] M. Akkurt, A.A. Khandar, M.N. Tahir, F.A. Afkhami, S.A.H. Yazdi, Acta Crystallogr., E E70 (2014) m213–m214.
[29] M. Abedi, O.Z. Yesilel, G. Mahmoudi, A. Bauza, S.E. Lofland, Y. Yerli, W. Kaminsky, P. Garczarek, J.K. Zareba, A. Ienco, A. Frontera, M.S. Gargari, Inorg. Chim. Acta 443 (2016) 101.
[30] M. Nishio, CrystEngComm 6 (2004) 130–158.
[31] A. Bauzá, A. Frontera, Angew. Chem., Int. Ed. 54 (2015) 7340–7343.